Global Energy Interconnection
Development and Cooperation Organization

ELSEVIER
Production And Hosting By Elsevier On Behalf Of KeAi
KeAi

Volume 4 Number 2 April 2021 (136-144)
DOI: 10.14171/j.2096-5117.gei.2021.02.003
Global Energy Interconnection
Contents lists available at ScienceDirect
https: //www.sciencedirect.com/journal/global-energy-interconnection

Full-length article

Multi-objective optimization for voltage and frequency control of smart grids based on controllable loads

Yaxin Wang, Donglian Qi, Jianliang Zhang
College of Electrical Engineering, Zhejiang University, Hangzhou 310027, P.R. China

Scan for more details

Abstract: The output uncertainty of high-proportion distributed power generation severely affects the system voltage and frequency. Simultaneously, controllable loads have also annually increased, which markedly improve the capability for nodal-power control. To maintain the system frequency and voltage magnitude around rated values, a new multi-objective optimization model for both voltage and frequency control is proposed. Moreover, a great similarity between the multi-objective optimization and game problems appears. To reduce the strong subjectivity of the traditional methods, the idea and method of the game theory are introduced into the solution. According to the present situational data and analysis of the voltage and frequency sensitivities to nodal-power variations, the design variables involved in the voltage and frequency control are classified into two strategy spaces for players using hierarchical clustering. Finally, the effectiveness and rationality of the proposed control are verified in MATLAB.

Keywords: Multi-objective optimization, Voltage control, Frequency control, Power flow, Controllable loads, Game theory.

0 Introduction

Recently, the penetration of renewable-energy power generation into distribution networks has rapidly increased for environmental reasons [1,2]. However, because of the randomness, intermittence, and volatility of the distributed power supply, severe are introduced into the system, including frequency collapse or voltage violation [3-5,10].

Meantime, the energy control capability has been enhanced following the use of smart end-user devices at the residential side. Therefore, voltage and frequency deviations can be controlled by these responsive end-user devices [6]. In [8-11], except for diesel generation, the demand side is also expected to reasonably provide voltage and frequency support. Electric vehicle (EV) is one of the typical controllable loads that can provide adequate reactive power at the distribution level to compensate for power imbalance [12]. To this end, EVs can be called upon to correct voltage deviations [13-16]. Similarly, thermostatically controllable loads, e.g., electric water heaters, air conditioners, and ground-source heat pumps, are ideal candidates to participate in primary frequency control [17,18]. The deviation in the system frequency is alleviated using electricity [14]. In contrast to the traditional instant load-cutting operation [19,20], the power consumption of controllable loads can be controlled without affecting the consumer comfort, and the load demand smoothly and continuously changes.

However, because of complex intercoupling among the

Received: November 16 2020 Accepted: February 18 2021 Published: April 25 2021

✉ Donglian Qi
qidl@zju.edu.cn

Jianliang Zhang
jlzhang@zju.edu.cn

Yaxin Wang
wangyaxin@zju.edu.cn

system frequency, nodal voltage, and active and reactive power [21-23], the aforementioned studies mainly focused on either voltage or frequency control. A multi-objective optimization framework for both voltage and frequency deviation correction has been lacking to fully employ the advantages of participating controllable loads, particularly in grids with high penetration of renewable-energy power.

Commonly, the solutions of multi-objective optimization problems are basically converted to a single-objective optimization problem by assigning weights to the targets [24,25]. Moreover, the selection of weighting factors is related to the importance of each goal, which is a difficult decision if no prior information is available for the problem to be solved [25]. Human factors greatly influence the weighting process; thus, this method suffers from the disadvantages of strong subjectivity [26]. Furthermore, other methods such as the sequencing and center methods are also based on reducing the dimension [27,28]. Similarly, the optimization process among the objectives is independent of one another [28,29]. Thus, the results are very inconsistent because of the lack of information exchange; thus, operators suffer from the difficulty of making effective decisions, and the process takes much time.

Currently, an increasing number of researchers are aware that a great similarity exists between the multi-objective optimization and game problems [30,31]. Game theory is an efficient method for solving multi-objective optimization problem [32,33]. In the present study, to solve the aforementioned problem, our contributions are focused on the following areas.

(a) A multi-objective optimization model is designed to minimize the effects of fluctuating power outputs from renewable-energy power generations, which provides a guide for controllable loads to deal with voltage- and frequency-deviation events.

(b) An optimization strategy for obtaining the optimal values of nodal-power variations is developed based on the Nash game to overcome the deficiency of subjectivities in the traditional methods.

1 Modeling of voltage and frequency sensitivities to nodal-power variations

In this section, the design of the generator, load, and power-flow models to analyze the sensitivity information of the voltage and frequency to nodal-power variations is presented.

1.1 Generator model

According to the active power–frequency characteristic curve shown in Fig. 1, the frequency deviation is considered in the generator model.

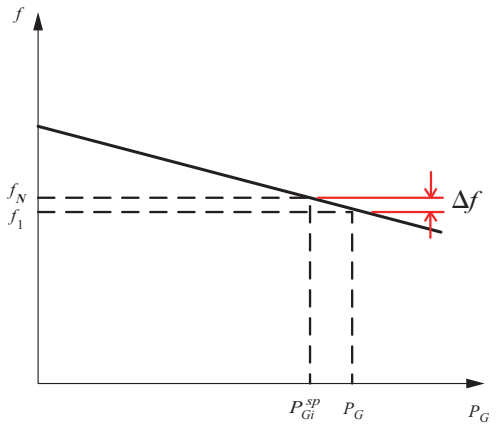

Fig. 1 Generator active power–frequency characteristic

$$\begin{aligned} P_{Gi} &= P_{Gi}^{sp} + \Delta P_{Gi} \\ \Delta P_{Gi} &= -K_{Gi}\Delta f \\ P_{Gi\_\min} &\leqslant P_{Gi} \leqslant P_{Gi\_\max} \end{aligned} \tag{1}$$

where P_{Gi}^{sp} is the active power specified at node i, ΔP_{Gi} is the deviation between the active power and specified value, K_{Gi} is the power-frequency characteristic coefficient of the generator at node i, and Δf is the deviation in the system frequency.

According to the generator reactive power-voltage characteristic curve shown in Fig. 2, the relationship between the reactive-power variations and generator terminal-voltage variations can be expressed as

$$\Delta Q_{G1} = -\frac{\Delta U_{Gi}}{\beta} \tag{2}$$

where ΔU_{Gi} is the generator terminal-voltage variations, ΔQ_{G1} is the generator reactive-power variations caused by ΔU_{Gi}, and β is the reactive power-voltage characteristic coefficient of the generator at node i.

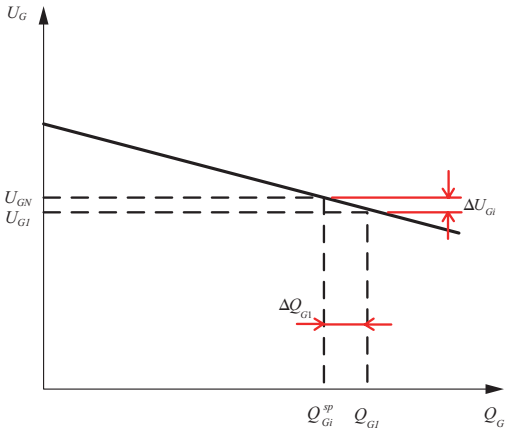

Fig. 2 Generator reactive power–voltage characteristic

Meanwhile, the reactive output power is also associated with active-power deviation ΔP_{Gi}; therefore, the actual reactive output power of the generator is adjusted according to (3), i.e.,

$$\begin{aligned} &Q_{Gi} = Q_{Gi}^{sp} + \Delta Q_{Gi} \\ &\Delta Q_{Gi} = \Delta Q_{G1} + a_Q \Delta P_{Gi} + b_Q \left(\Delta P_{Gi}\right)^2 \\ &Q_{Gi\_\min} \leqslant Q_{Gi} \leqslant Q_{Gi\_\max} \end{aligned} \tag{3}$$

where Q_{Gi}^{sp} is the reactive power specified at node i, ΔQ_{Gi} is the deviation between the reactive power and specified value, and a_Q and b_Q are the coefficients of reactive-power generation control characteristics.

1.2 Load model

By considering the effects of the system frequency deviation and nodal voltage magnitude, the active and reactive power of the loads can be expressed as follows:

$$\begin{aligned} P_{Li} &= P_{Li}^{sp}\left(1 + K_{pi}\Delta f\right)\left(p_{pi} + p_{ci}\left(\frac{U^{sp}}{V_{LB}}\right) + p_{zi}\left(\frac{U^{sp}}{V_{LB}}\right)^2\right) \\ Q_{Li} &= Q_{Li}^{sp}\left(1 + K_{Qi}\Delta f\right)\left(q_{pi} + q_{ci}\left(\frac{U^{sp}}{V_{LB}}\right) + q_{zi}\left(\frac{U^{sp}}{V_{LB}}\right)^2\right) \end{aligned} \tag{4}$$

where P_{Li}^{sp} is the load active power specified at node i, Q_{Li}^{sp} is the load reactive power specified at node i, K_{pi} and K_{Qi} are respectively the active and reactive-power-frequency characteristic coefficients of the load, p_{pi}, p_{ci}, p_{zi}, q_{pi}, q_{ci}, and q_{zi} are the active-and reactive-power-voltage characteristic coefficients of the load, U^{sp} is the specified terminal voltage, and V_{LB} is the voltage magnitude at the node connected to the load.

1.3 Power-flow model

The active and reactive power injected at bus i can be expressed in polar form as follows:

$$\begin{aligned} P_i &= \sum_{j=1}^{n} U_i U_j \left(G_{ij}\cos\theta_{ij} + B_{ij}\sin\theta_{ij}\right) \\ Q_i &= \sum_{j=1}^{n} U_i U_j \left(G_{ij}\sin\theta_{ij} - B_{ij}\cos\theta_{ij}\right) \end{aligned} \tag{5}$$

where U_i and U_j are the voltage magnitude at nodes i and j, respectively, $G_{ij}+jB_{ij}$ is the element of the system admittance at row i and column j, and θ_{ij} is the nodal phase difference between nodes i and j.

Once the power generation and consumption in the system become imbalance, the frequency deviates from the normal value. As discussed in the generator and load models, the active- and reactive-power mismatches are represented as functions of the state variables $(\Delta f, \theta, U)$, which are equal to zero when the system reaches a new stable equilibrium point.

$$\begin{aligned} \Delta P_i &= P_{Gi} - P_{Li} - P_i = 0 \\ \Delta Q_i &= Q_{Gi} - Q_{Li} - Q_i = 0 \end{aligned} \tag{6}$$

These nonlinear power-flow equations are usually iteratively solved using the Newton–Raphson method until $|\Delta P| < \varepsilon$, $|\Delta Q| < \varepsilon$. The relationship between the power mismatches and state variable modifications can be expressed by Jacobian matrix $\mathbf{J}_{\mathbf{ext}}$.

$$-\begin{bmatrix} \mathbf{\Delta P} \\ \mathbf{\Delta Q} \end{bmatrix} = \mathbf{J}_{\mathbf{ext}} \begin{bmatrix} \Delta(\Delta f) \\ \mathbf{\Delta\theta} \\ \mathbf{\Delta U} \end{bmatrix} \tag{7}$$

$$\mathbf{J}_{\mathbf{ext}} = \begin{bmatrix} \dfrac{\partial \mathbf{\Delta P}}{\partial \Delta f} & \dfrac{\partial \mathbf{\Delta P}}{\partial \mathbf{\theta}} & \dfrac{\partial \mathbf{\Delta P}}{\partial \mathbf{U}} \\ \dfrac{\partial \mathbf{\Delta Q}}{\partial \Delta f} & \dfrac{\partial \mathbf{\Delta Q}}{\partial \mathbf{\theta}} & \dfrac{\partial \mathbf{\Delta Q}}{\partial \mathbf{U}} \end{bmatrix} \tag{8}$$

where $\mathbf{\Delta P}$ and $\mathbf{\Delta Q}$ are the variable sets of the active- and reactive-power mismatches at each node, respectively, $\Delta(\Delta f)$ is the modification in the system frequency deviation, $\mathbf{\Delta\theta}$ is the variable set of nodal phase modifications, and $\mathbf{\Delta U}$ is the variable set of nodal voltage-magnitude modifications.

Alternatively, when the nodal active and reactive power is adjusted, changes occur in the system frequency and nodal voltage levels. In addition, the mathematical relationship can be obtained based on the power-flow functions.

$$-\begin{bmatrix} \Delta(\Delta f) \\ \mathbf{\Delta\theta} \\ \mathbf{\Delta U} \end{bmatrix} = \left[\mathbf{J}_{\mathbf{ext}}\right]^{-1} \begin{bmatrix} \mathbf{\Delta P} \\ \mathbf{\Delta Q} \end{bmatrix} = \begin{bmatrix} \dfrac{\partial \Delta f}{\partial \mathbf{\Delta P}} & \dfrac{\partial \Delta f}{\partial \mathbf{\Delta Q}} \\ \dfrac{\partial \mathbf{\theta}}{\partial \mathbf{\Delta P}} & \dfrac{\partial \mathbf{\theta}}{\partial \mathbf{\Delta Q}} \\ \dfrac{\partial \mathbf{U}}{\partial \mathbf{\Delta P}} & \dfrac{\partial \mathbf{U}}{\partial \mathbf{\Delta Q}} \end{bmatrix} \begin{bmatrix} \mathbf{\Delta P} \\ \mathbf{\Delta Q} \end{bmatrix} \tag{9}$$

where $\dfrac{\partial \Delta f}{\partial \mathbf{\Delta P}}$ and $\dfrac{\partial \Delta f}{\partial \mathbf{\Delta Q}}$ are the sensitivities of Δf to $\mathbf{\Delta P}$ and $\mathbf{\Delta Q}$, respectively, $\dfrac{\partial \mathbf{\theta}}{\partial \mathbf{\Delta P}}$ and $\dfrac{\partial \mathbf{\theta}}{\partial \mathbf{\Delta Q}}$ are the sensitivities of $\mathbf{\theta}$ to $\mathbf{\Delta P}$ and $\mathbf{\Delta Q}$, respectively, and $\dfrac{\partial \mathbf{U}}{\partial \mathbf{\Delta P}}$ and $\dfrac{\partial \mathbf{U}}{\partial \mathbf{\Delta Q}}$ are the sensitivities of $\mathbf{U}$ to $\mathbf{\Delta P}$ and $\mathbf{\Delta Q}$, respectively.

2 Multi-objective optimization framework for voltage and frequency control

A multi-objective optimization model is designed for controllable loads to participate in the voltage and frequency control, as presented in this section.

Design variables

Participation of responsive end-user devices in voltage

and frequency control can be realized by supporting the nodal-power variations. Therefore, both ΔP_i and ΔQ_i of node i are design variables.

Objective functions

The characteristics of randomness, intermittence, and volatility of distributed generations lead to generation–consumption imbalance, which aggravates the frequency and nodal voltage deviation in the system.

$$F_1 = \min \sum_{i=1}^{n} \left| U_i - U^* \right| \tag{10}$$

where U_i is the actual voltage magnitude at node i and U^* is the standard voltage magnitude of the system.

According to the sensitivities of **U** to **ΔP** and **ΔQ**, ΔU_i can be expressed as

$$-\Delta U_i = \sum_{j=1}^{n} \left(\frac{\partial U_i}{\partial \Delta P_j} \Delta P_j + \frac{\partial U_i}{\partial \Delta Q_j} \Delta Q_j \right) \tag{11}$$

Therefore, U_i is a function of design variables ΔP_j and ΔQ_j $(j = 1, 2..., n)$.

$$U_i = U_{i0} - \Delta U_i = U_{i0} - \sum_{j=1}^{n} \left(\frac{\partial U_i}{\partial \Delta P_j} \Delta P_j + \frac{\partial U_i}{\partial \Delta Q_j} \Delta Q_j \right) \tag{12}$$

where U_{i0} is the voltage magnitude at node i before the control.

To minimize the frequency deviation in the system, another objective function can be expressed as

$$F_2 = \min \left| f - f^* \right| \tag{13}$$

where f is the system frequency after the control and f^* is the standard frequency magnitude.

Similarly, by deriving ΔU_i, $\Delta(\Delta f)$ can be expressed as follows with sensitivities of Δf to **ΔP** and **ΔQ**:

$$-\Delta(\Delta f) = \sum_{i=1}^{n} \frac{\partial \Delta f}{\partial \Delta P_i} \Delta P_i + \frac{\partial \Delta f}{\partial \Delta Q_i} \Delta Q_i \tag{14}$$

Then

$$f - f^* = \Delta f_0 - \Delta(\Delta f) = \Delta f_0 - \sum_{i=1}^{n} \frac{\partial \Delta f}{\partial \Delta P_i} \Delta P_i + \frac{\partial \Delta f}{\partial \Delta Q_i} \Delta Q_i \tag{15}$$

Therefore, F_2 is also a function of design variables ΔP_j and ΔQ_j $(j = 1, 2..., n)$.

Constraint conditions

Because the nodal load power cannot be freely adjusted, constraints exist in both ΔP_i and ΔQ_i, which are not allowed to exceed the upper limits.

3 Game analysis methods of multi-objective problem

3.1 Strategy space of game players

A large similarity exists between the multi-objective optimization and game problems. Therefore, the idea and method of the game theory are introduced into the multi-objective optimization to overcome the disadvantages of the traditional methods, such as reducing the strong subjectivity.

Players

P_1 and P_2 are considered as two participants in the multi-objective optimization problem. P_1 wishes to minimize the sum of the nodal voltage-magnitude deviation, and P_2 wishes to minimize the system frequency deviation.

Strategy space

The strategy space consists of design variables ΔP_i and ΔQ_i proposed in the multi-objective optimization problem.

$$X = \left\{ x_1, x_2 ..... x_{2n} \right\} = \left\{ \Delta P_1, \Delta P_2 ..... \Delta P_n, \Delta Q_1, \Delta Q_2 ..... \Delta Q_n \right\}$$

Utility functions

The utility functions of the players can be designed as the objection functions proposed in the previous section.

$$u_i(X_i) = F_i(X_i)$$

3.2 Nodal-power-variation optimization

Step 1: Finding the optimal solution of each single objective

Two single objective functions are optimized, and optimal solution $F_1\left(X_1^*\right), F_2\left(X_2^*\right)$, where $X_i^* = \left\{ x_{1i}^*, \ x_{2i}^*, \ \cdots, \ x_{2ni}^* \right\}, (i = 1, 2)$ are then obtained.

Step 2: Calculating the impact factor

Δ_{ji} represents the impact factor of variable j on single objective i, which can be expressed as

$$\Delta_{ji} = \frac{1}{F_i} \times \left. \frac{\partial F_i \left(x_{1i}^*, \cdots, x_{(j-1)i}^*, x_j, x_{(j+1)i}^*, \cdots, x_{2ni}^* \right)}{\partial x_j} \right|_{x_j = x_{ji}^*} \tag{16}$$

$(i = 1, 2; j = 1, 2, \cdots, 2n)$

For convenience, $\boldsymbol{\Delta}_j (\boldsymbol{\Delta}_j = \{\Delta_{j1}, \Delta_{j2}\})$ includes the impact factors of variable j on each objective.

$$\boldsymbol{\Delta} = \left\{ \boldsymbol{\Delta}_1, \boldsymbol{\Delta}_2, \cdots, \boldsymbol{\Delta}_{2n} \right\} \tag{17}$$

Then, the impact factors are analyzed using hierarchical clustering.

The impact factors are divided into two classes according to the number of optimization targets. The strategy sets of the corresponding participants are generated according to the average value of each class of impact factors on each objective function.

$$S_1 \cup S_2 = \left\{ x_1, x_2, ..., x_{2n} \right\}$$

where S_1 and S_2 are the strategy sets for Players 1 and 2, respectively.

Step 3: Optimization process based on the Nash equilibrium model

Each player randomly selects the initial values of the design variables from their own strategy spaces $s_1^{(0)}$ and $s_2^{(0)}$, which generate $s^{(0)}$ as the initial feasible strategy.

$$s^{(0)} = s_1^{(0)} \cup s_2^{(0)} = \left\{ x_1^{(0)}, x_2^{(0)}, ..., x_{2n}^{(0)} \right\}$$

Let $\bar{s}_1^{(0)}, \bar{s}_2^{(0)}$ be the complement sets of $s_1^{(0)}, s_2^{(0)}$ in strategy set $s^{(0)}$.

For player i, $\bar{s}_i^{(0)}$ is fixed. The particle swarm optimization (PSO) is used to solve best strategy s_i^* for Player i; actually, other methods can also be used [34], which satisfies

$$u_i(s_i^*, \bar{s}_i^{(0)}) \leqslant u_i(s_i, \bar{s}_i^{(0)})$$

Therefore

$$\min F_i(s_i, \bar{s}_i^{(0)}) = u_i(s_i^*, \bar{s}_i^{(0)})$$

For two players, each player uses its own utility function as the goal and carries out single objective optimization in his own strategy space to obtain the best strategy in reply to the other player.

The union set of s_i^* for each player forms new strategy set $s^{(1)} = s_1^* \cup s_2^*$ and then calculates norm $\left\| s^{(1)} - s^{(0)} \right\|$ between strategy sets $s^{(1)}$ and $s^{(0)}$.

(a) If $\left\| s^{(1)} - s^{(0)} \right\| > \varepsilon$ (ε is a fixed positive number), the convergence condition is not satisfied. Strategy set $s^{(0)}$ is updated as $s^{(0)} = s^{(1)}$. Then, the process returns, and ***step3*** is repeated until the convergence condition is satisfied.

(b) If $\left\| s^{(1)} - s^{(0)} \right\| \leqslant \varepsilon$, this condition signifies that the algorithm converges. s_1^* represents the best strategy for Player 1 to reply to Player 2, and s_2^* represents the best strategy for Player 2 to reply to Player 1. Then, the game ends.

According to the definition of Nash equilibrium in the game, if strategy s_i^* of arbitrary Player i is the best strategy to reply to all other players, the following exists for any $s_{ij} \in S_i$:

$$u_i(s_1^*, ..., s_i^*, ..., s_m^*) \leqslant u_i(s_1^*, ..., s_{ij}, ..., s_m^*) \tag{18}$$

Then, strategy set $(s_1^*, ..., s_i^*, ..., s_m^*)$ is called a Nash equilibrium. Hence, $s^{(1)} = s_1^* \cup s_2^*$ presented in this section is a Nash equilibrium, which is also the optimal solution of the multi-objective problem.

4 Case studies

The test system is an improved IEEE33 node distribution network shown in Fig. 3, whose detailed information is presented in [35]. It consists of 32 branches and three distributed generations (DG) with a capacity of 240 kW. The reference value of the nodal voltage is 12.66 kV, and the total load of the system is 3715 + *j*2300 kVA.

A variation in the distributed generation output power occurs due to external environment. In this part, the variation in the power output of each DG is assumed to increase by 10%.

Two specific objective functions are present with the participation of responsive end-user devices in the voltage and frequency control, as mentioned in Section 3.

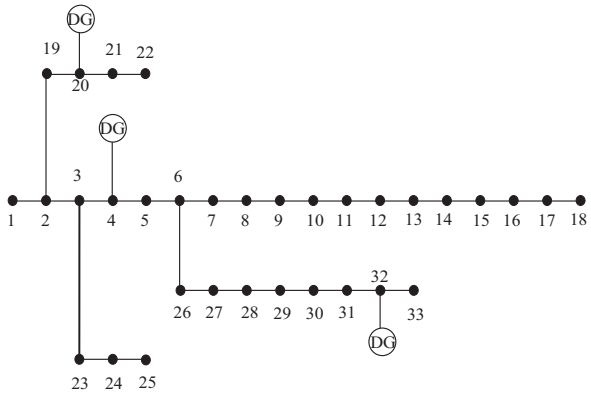

Fig. 3 Improved IEEE33 node distribution network

We set the controllable load capacity of all nodes to ±20% of both their load active and reactive power. Therefore, the load power variations at each node are all design variables, which are listed as follows:

$$X = \{x_1, x_2 ..... x_{2\times 33}\} = \{\Delta P_1, \Delta P_2 ..... \Delta P_{33}, \Delta Q_1, \Delta Q_2 ..... \Delta Q_{33}\}$$

$$\begin{cases} \Delta P_i \leqslant 0.2 \times P_{Li} \\ \Delta Q_i \leqslant 0.2 \times Q_{Li} \end{cases} (i = 1, 2, ..., 33)$$

We then calculate their impact factors for every objective function.

$$\boldsymbol{\Delta}_j = \{\Delta_{j1}, \Delta_{j2}\}_{(j=1,2,...,2\times 33)}$$

For all vectors $\boldsymbol{\Delta}_j (j = 1, 2, ..., 2 \times 33)$, the first part represents the impact factor of Player 1, and the second part represents the impact factor of Player 2. Then, these design variables are analyzed using hierarchical clustering. The strategy spaces of Players 1 and 2 can be obtained, as shown in Fig. 4.

Fig. 4 shows that the longest distance between the impact factors of similarity decision is set as 0.95. Obviously, the design variables can be clustered into two groups.

According to the multi-objective optimization strategy proposed in Section 4, to obtain the best strategy for each player in the game iterations, the particle swarm population size is set to 50, the learning factors are set as $c_1 = c_2 = 0.5$, and the inertial weight is set as $w = 0.8$.

The calculation processes of the voltage and frequency indexes converge within several generations, as shown in Figs. 5 and 6, respectively.

During the final iteration of the game, the curve-analysis results verify that the voltage index converges to 13.0625, and the frequency deviation converges to almost zero.

Table 1 illustrates the results of the optimal active/reactive power variations in each node. The nodal voltages of the system before and after the control for the considered event are shown in Fig. 7, which reveals a voltage profile closed to the standard line result with the application of the proposed strategy.

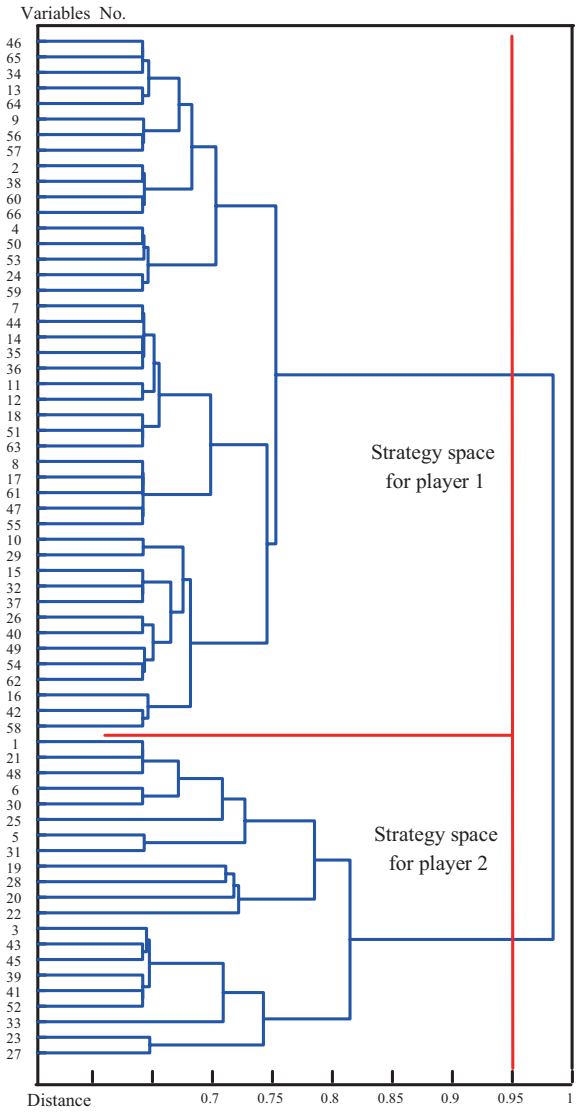

Fig. 4 Cluster tree of the design variables

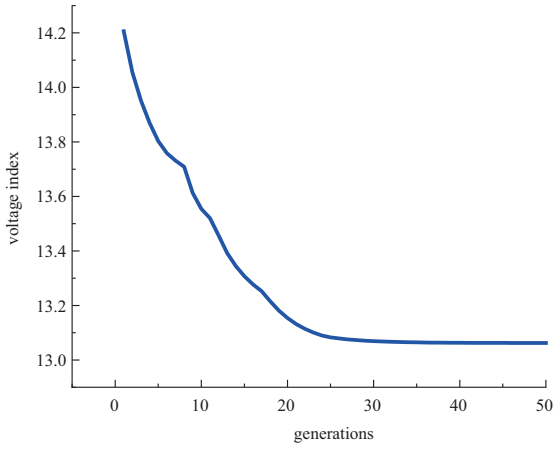

Fig. 5 Optimization process of the voltage index in the final iteration

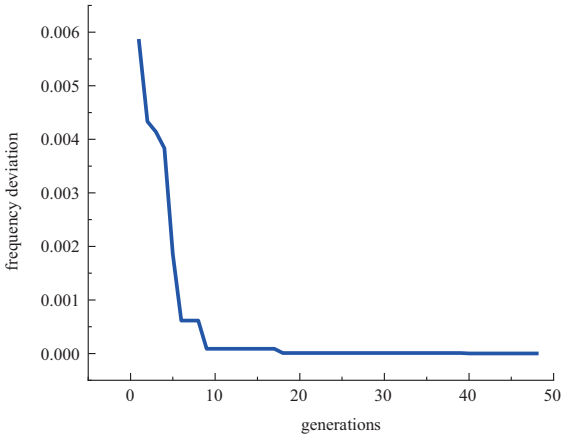

Fig. 6 Optimization process of the frequency deviation in the final iteration

Table 1 Results of the active/reactive power variations

Node no.	Active-power variations	Reactive-power variations
No. 2	−5.98386	−8.73998
No. 3	6.23417	−0.49973
No. 4	−13.3161	−16.1515
No. 5	5.69672	−7.1892
No. 6	1.27682	6.75853
No. 7	−3.27649	−31.457
No. 8	−39.3955	2.02932
No. 9	−0.3215	−5.28779
No. 10	−1.5294	−10.1608
No. 11	−7.57553	−7.965
No. 12	−24.0995	2.23505
No. 13	−9.80878	−9.98604
No. 14	−27.5424	−3.82206
No. 15	10.2866	2.63124
No. 16	12.5324	−3.84314
No. 17	4.41175	−0.36217
No. 18	1.73925	−18.3561
No. 19	−3.23326	5.33428
No. 20	10.2833	−2.06109
No. 21	5.04868	−2.53856
No. 22	4.58371	−15.5698
No. 23	7.20289	−10.5872
No. 24	−15.2199	−8.88365
No. 25	40.496	−13.7804
No. 26	0.820216	2.51217
No. 27	7.46986	−10.5199
No. 28	12.0432	4.3969
No. 29	4.66824	−9.56736
No. 30	−16.919	−38.5315
No. 31	−11.8428	−17.0591
No. 32	−25.8633	−11.8346
No. 33	5.27084	−3.91142

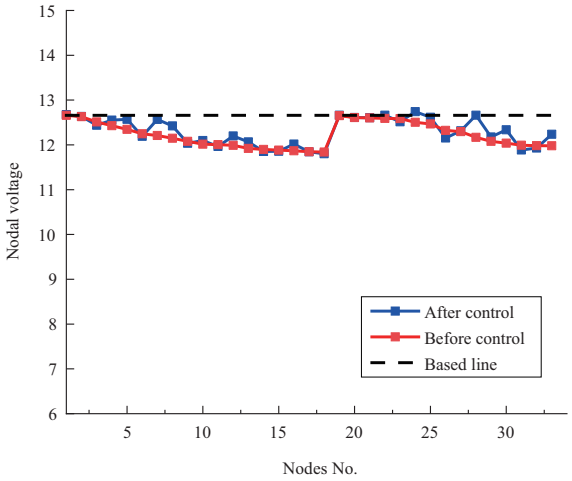

Fig. 7 Nodal voltage of the system before and after the control

The comparisons of the voltage index and system frequency before and after the control are listed in Table 2.

Table 2 Results of the voltage and frequency control

	Index	Before the control	After the control
Proposed Control	Frequency	50.0239 Hz	50.0000 Hz
	Voltage index	14.3880	13.06250
Traditional Control	Frequency	50.0239 Hz	50.0233 Hz
	Voltage index	14.3880	13.05812

The results listed in Table 2 illustrate that both index values have been optimized under the proposed control. In addition, the proposed method avoids the effect of the magnitude of the different objective functions and eliminates subjectivity. As a result, compared with the traditional method that is based on weighting targets, the proposed method not only improves the nodal voltage level but also markedly reduces the system frequency deviation. The effectiveness and rationality of the proposed control are then verified.

5 Conclusion

Existing approaches do not consider the potential power-conditioning ability of controllable loads. To deal with the voltage and frequency deviations caused by renewable-power sources, the multi-objective optimization model, which involves both nodal voltage and system frequency, is proposed based on responsive end-user devices. In addition, to obtain optimal nodal-power variations due to power-output disturbances from distributed generations, an optimization strategy is developed under the Nash game framework. Under the proposed strategy, the controllable loads are utilized to optimize the nodal-power variations. The simulation results indicate that the proposed control is effective when a sudden variation in the distributed generation output power occurs. Not only the nodal voltage level improves but also the system frequency deviation is markedly reduced. With the development of smart grids, the works presented in this paper can help in guiding the demand side support the voltage and frequency.

Acknowledgements

This work was supported by the National Key Research and Development Program of China (Basic Research Class) (No. 2017YFB0903000) and the National Natural Science Foundation of China (No. U1909201).

Declaration of Competing Interest

We have no conflict of interest to declare.

References

[1] Altaf M W, Arif M T, Saha S et al (2020) Renewable energy integration challenge on power system protection and its mitigation for reliable operation. IECON 2020 The 46th Annual Conference of the IEEE Industrial Electronics Society. Singapore. IEEE, 1917-1922

[2] Xu Q Y, Mao T, Wang J Y et al (2019) A business framework for distributed power demand and storage response with the maximization of renewable energy accommodation. 2019 IEEE Power & Energy Society General Meeting (PESGM), Atlanta, GA, USA, 2019, 1-5

[3] Wang J L, Li J (2019) Effect of integration of wind and photovoltaic power on Henan power grid steady-state. Power System and Clean Energy, 35(9): 81-87

[4] X. H. Yang, J. B. Luo, C. Yu, et al (2020) Review of power system reserve configuration and optimization for large-scale renewable energy integration. Electric Power Engineering Technology, 2020,39(1): 10-20,63

[5] Ferreyra D, Sarmiento C, Reineri C (2013) Harmonic state estimation on a radial distribution system with distributed generation. IEEE Latin America Transactions, 11(1): 499-504

[6] Tokudome M, Tanaka K, Senjyu T et al (2009) Frequency and voltage control of small power systems by decentralized controllable loads. 2009 International Conference on Power Electronics and Drive Systems (PEDS). Taipei, Taiwan, China. IEEE, 666-671

[7] Y. Chen, X. Cao, J. Wang, et al (2020) Integrated demand response behavior of integrated energy system. Electric Power Engineering Technology, 2020,39(6):89-97

[8] Huang W, Yan Y W, Li H et al (2020) Research on planning

of distributed photovoltaic power supply connected to medium voltage distribution network under the condition of satisfying voltage quality. 2020 IEEE Sustainable Power and Energy Conference (iSPEC). Chengdu, China. IEEE, 355-362

[9] Khalil A, Rajab Z (2017) Load frequency control system with smart meter and controllable loads. 2017 8th International Renewable Energy Congress (IREC), 1-6

[10] Munikoti S, Natarajan B, Jhala K et al (3461) Probabilistic voltage sensitivity analysis to quantify impact of high PV penetration on unbalanced distribution system. IEEE Transactions on Power Systems, PP(99): 1

[11] J. Shen, J. Wang, F. Xiong, et al (2020) Load-shedding control strategy of microgrid based on smart loads. Electric Power Engineering Technology, 2020,39(2): 103-109

[12] Takahashi A, Matsumoto N, Imai J et al (2017) A voltage control method using EVs in the power distribution system including a mass of PVs. 2017 IEEE 12th International Conference on Power Electronics and Drive Systems (PEDS). Honolulu, HI, 507-510

[13] Pourmousavi S A, Nehrir M H (2013) Real-time central demand response for primary frequency regulation in microgrids. IEEE Transactions on Smart Grid. IEEE, 1988-1996

[14] Cecati C, Citro C, Siano P (2011) Combined operations of renewable energy systems and responsive demand in a smart grid. IEEE Transactions on Sustainable Energy, 2(4): 468-476

[15] M.Kamgarpour, C. Ellen, S. E. Z. Soundjani, et al (2013) Modeling options for demand side participation of thermostatically controlled loads. In: Proceedings of the Symposium. Bulk Power System. Dynamics and Control (IREP), Rethymnon, Greece, August 2013

[16] Samarakoon K, Ekanayake J, Jenkins N (2012) Investigation of domestic load control to provide primary frequency response using smart meters. IEEE Transactions on Smart Grid, 3(1): 282-292

[17] Y. Kinjyo, M. D. Palmer, A. Yona, et al (2013) Autonomous power system control by decentralized controllable loads. In: Proceedings of the 2013 IEEE 10th International Conference on Power Electronics and Drive Systems (PEDS), Kitakyushu, Japan,IEEE, 881-886

[18] X. Chen, C. Lu, Y. Han (2020). Review of power system frequency problems and frequency dynamic characteristics. Electric Power Engineering Technology, 2020,39(1):1-9

[19] Zhang Y C, Wu W C, Lu Q Y et al (2018) Security-based load shedding strategy considering the load frequency dependency in island distribution system. In: Proceedings of the 2018 2nd IEEE Conference on Energy Internet and Energy System Integration (EI2). Beijing. IEEE, 1-6

[20] Wang Y M, Wang Y, Ding Y et al (2019) A fast load-shedding algorithm for power system based on artificial neural network. 2019 International Conference on IC Design and Technology (ICICDT). Suzhou, China. IEEE, 1-4

[21] Bayat M, Sheshyekani K, Rezazadeh A (2015) A unified framework for participation of responsive end-user devices in voltage and frequency control of the smart grid. IEEE Transactions on Power Systems, 30(3): 1369-1379

[22] Meng R, Ye Y, Xie N G (2010) Multi-objective optimization design methods based on game theory. In: Proceedings of the 2010 8th World Congress on Intelligent Control and Automation, Jinan, China, 2220-2227

[23] Okamura M, O-Ura Y, Hayashi S et al (1975) A new power flow model and solution method-Including load and generator characteristics and effects of system control devices. IEEE Transactions on Power Apparatus and Systems, 94(3): 1042-1050

[24] Nazim CHEBOUBA B, Arezki MELLAL M, Adjerid S et al (2020) Multi-objective system reliability-redundancy allocation in a power plant by considering three targets. In: Proceedings of the 2020 7th International Conference on Control, Decision and Information Technologies (CoDIT). Prague, Czech Republic. IEEE, 674-678

[25] Zhao W, Qi L, Sun X F et al (2016) Research on dual optimization control scheme considering voltage and frequency in islanding microgrid. In: Proceedings of the 2016 IEEE 8th International Power Electronics and Motion Control Conference (IPEMC-ECCE Asia). Hefei, China. IEEE, 3163-3168

[26] Su X J, Masoum M A S, Wolfs P (2014) PSO based multi-objective optimization of unbalanced lv distribution network by PV inverter control. In: Proceedings of the 2014 China International Conference on Electricity Distribution (CICED). Shenzhen, China. IEEE, 1744-1748

[27] Tan S W, Lin S J, Yang L Q et al (2013) Multi-objective optimal power flow model for power system operation dispatching. In: Proceedings of the 2013 IEEE PES Asia-Pacific Power and Energy Engineering Conference (APPEEC). Hong Kong, China. IEEE, 1-6

[28] Kang X N, Ma X D, Wang H et al (2016) Multi-objective optimal power flow for DC distribution system. In: Proceedings of the 2016 China International Conference on Electricity Distribution (CICED). Xi'an, China. IEEE, 1-5

[29] H.Yan, L. Kang, D. Zhou (2019) Optimal Model of Day-Ahead Dispatching and Energy Storage for Micro-Grid Considering Randomness. Power System and Clean Energy, 2019, 35(11): 61-65

[30] Ma J, Li P, Lin X P et al (2015) Game theory method for multi-objective optimizing operation in microgrid. In: Proceedings of the 2015 IEEE 12th International Conference on Networking, Sensing and Control. Taipei, Taiwan, China. IEEE, 421-425

[31] M. Yang, J. Wangi (2020) Multi-Objective Optimization Scheduling of Islanded Microgrid Participated by Demand Management[J]. Power System and Clean Energy, 2020, 36(1): 1-12

[32] Xu Y T, Ai Q (2015) Integrated optimization of distribution network incorporating microgrid based on co-evolutionary game algorithm. In: Proceedings of the International Conference on Renewable Power Generation (RPG 2015). Beijing. IET, 1-6

[33] Qin Y J, Wu L L, Zheng J H et al (2019) Optimal operation of integrated energy systems subject to coupled demand constraints of electricity and natural gas. CSEE Journal of Power and Energy Systems, 6(2): 444-457

[34] You. Guangzeng, Hang. Zhi, Chen Kai, et al (2020) Wind turbine

generator frequency control based on improved particle swarm optimization. Electric Power Engineering Technology, 39(3): 43-50

[35] Kashem M A, Ganapathy V, Jasmon G B et al (2000) A novel method for loss minimization in distribution networks. In: Proceedings of the DRPT2000. International Conference on Electric Utility Deregulation and Restructuring and Power Technologies. Proceedings (Cat. No.00EX382). London, UK. IEEE, 251-256

Biographies

Yaxin Wang received B.E. degree at Zhengzhou University, Zhengzhou, China, in 2019. She is currently pursuing the Ph.D degree with the College of Electrical Engineering, Zhejiang University, Hangzhou, China. Her current research interests include voltage and frequency optimization control in smart grid, and game theory and distributed optimization, with applications to power systems.

Donglian Qi received the Ph.D. degree in control theory and control engineering from Zhejiang University, Hangzhou, China, in March 2002. Since then, she has been with the College of Electrical Engineering, Zhejiang University where she is currently a Professor. Her research interests include the basic theory and application of cyber physical power system (CPPS), digital image processing, artificial intelligence, and electric operation and maintenance robots. She is an Editor for the Clean Energy, the IET Energy Conversion and Economics, and the Journal of Robotics, Networking and Artificial Life.

Jianliang Zhang received his Ph.D degree in control theory and control engineering from Zhejiang University, Hangzhou, China, in June 2014. Since then, he has been working with College of Electrical Engineering, Zhejiang University(ZJU). He was a visiting scholar at Hongkong Polytechnic University(PolyU) (2016-2017). His current research interests include distributed optimization, with applications to energy/ power systems, and cyber-physical security with application in smart grid, etc.

(Editor Dawei Wang)